Physics of the Earth and Planetary Interiors 169 (2008) 140–151

Contents lists available at ScienceDirect

Physics of the Earth and Planetary Interiors

journal homepage: www.elsevier.com/locate/pepi

Origin of orbital periods in the sedimentary relative paleointensity records

Chuang Xuan*, James E.T. Channell

Department of Geological Sciences, University of Florida, 241 Williamson Hall, P.O. Box 112120, Gainesville, FL 32611, United States

ARTICLE INFO

Article history:
Received 31 December 2007
Received in revised form 15 July 2008
Accepted 15 July 2008

Keywords:
Geomagnetic paleointensity
Orbital periods
Wavelet analysis

ABSTRACT

Orbital cycles with 100 kyr and/or 41 kyr periods, detected in some sedimentary normalized remanence (relative paleointensity) records by power spectral analysis or wavelet analysis, have been attributed either to orbital forcing of the geodynamo, or to lithologic contamination. In this study, local wavelet power spectra (LWPS) with significance tests have been calculated for seven relative paleointensity (RPI) records from different regions of the world. The results indicate that orbital periods (100 kyr and/or 41 kyr) are significant in some RPI records during certain time intervals, and are not significant in others. Time intervals where orbital periods are significant are not consistent among the RPI records, implying that orbital periods in these RPI records may not have a common origin such as orbital forcing on the geodynamo. Cross-wavelet power spectra (|XWT|) and squared wavelet coherence (WTC) between RPI records and orbital parameters further indicate that common power exists at orbital periods but is not significantly coherent, and exhibits variable phase relationships, implying that orbital periods in RPI records are not caused directly by orbital forcing. Similar analyses for RPI records and benthic oxygen isotope records from the same sites show significant coherence and constant in-phase relationships during time intervals where orbital periods were significant in the RPI records, indicating that orbital periods in the RPI records are most likely due to climatic 'contamination'. Although common power exists at orbital periods for RPI records and their normalizers with significant coherence during certain time intervals, phase relationships imply that 'contamination' (at orbital periods) is not directly due to the normalizers. Orbital periods are also significant in the NRM intensity records, and 'contamination' in RPI records can be attributed to incomplete normalization of the NRM records. Further tests indicate that 'contamination' is apparently not directly related to physical properties such as density or carbonate content, or to the grain size proxy κ_{ARM}/κ. However, WTC between RPI records and the grain size proxy ARM/IRM implies that ARM/IRM does reflect the 'contamination' in some RPI records. It appears that orbital periods were introduced into the NRM records (and have not been normalized when calculating RPI records) through magnetite grain size variations reflected in the ARM/IRM grain size proxy. The orbital power in ARM/IRM for some North Atlantic sites is probably derived from bottom-current velocity variations that are orbitally modulated and are related to the vigor of thermohaline circulation and the production of North Atlantic Deep Water (NADW). In the case of ODP Site 983, the orbital power in RPI appears to exhibit a shift from 41-kyr to 100-kyr period at the mid-Pleistocene climate transition (~750 ka), reinforcing the climatic origin of these orbital periods. RPI records from the Atlantic and Pacific oceans, and RPI records with orbital periods eliminated by band-pass filters, are highly comparable with each other in the time domain, and are coherent and in-phase in time-frequency space, especially at non-orbital periods, indicating that 'contamination', although present (at orbital periods) is not debilitating to these RPI records as a global signal that is primarily of geomagnetic origin.

Published by Elsevier B.V.

1. Introduction

The possible connection between the geomagnetic field and orbital parameters has been controversial for nearly 60 years. Geodynamos driven by precessional forces were discussed by Bullard (1949) and were then advocated in the 1960s (e.g. Malkus, 1968). Theoretical studies by Rochester et al. (1975) and Loper (1975), based on the energetics of laminar flow conditions, however, concluded that the energy available from precession is insufficient to drive the geodynamo. Since then, Gubbins and Roberts (1987) and Kerswell (1996) considered turbulent dissipation and suggested that the energy due to orbital precession could be of the order required to power the geodynamo. More recent theoreti-

* Corresponding author. Tel.: +1 352 392 2231; fax: +1 352 392 9294.
E-mail addresses: xuan2005@ufl.edu (C. Xuan), jetc@geology.ufl.edu (J.E.T. Channell).

0031-9201/$ – see front matter. Published by Elsevier B.V.
doi:10.1016/j.pepi.2008.07.017

cal (e.g. Christensen and Tilgner, 2004; Tilgner, 2005, 2007; Wu and Roberts, 2008) and experimental work (e.g. Vanyo and Dunn, 2000) have been interpreted to favor the possibility of a precessionally powered geodynamo. Orbital forcing has not been taken into account in numerical simulations of the geodynamo (Glatzmaier and Roberts, 1996; Glatzmaier et al., 1999) in part because the time step in any precession model is necessarily so small that useful simulations require unreasonably long run times, which taxes even high-speed computers.

By comparing the timing of reversals with orbital solutions over the last few million years, Fuller (2006) proposed a link between orbital obliquity and polarity reversal, thereby providing further evidence of orbital forcing of the geodynamo. Kent and Carlut (2001), however, found no discernable tendency for reversals or excursions to occur at a consistent amplitude or phase of obliquity or eccentricity. A recent analysis over a longer time period also failed to confirm such a relationship and pointed out that imprecision in current polarity timescales does not, at present, allow a relationship to be firmly established between reversal age and orbital obliquity or orbital eccentricity (Xuan and Channell, 2008).

Normalized records of sedimentary natural remanent magnetization (NRM) are often interpreted as representing the relative paleointensity (RPI) of the geomagnetic field, and criteria have been proposed for selecting sediments suitable for paleointensity determinations (Johnson et al., 1948; Levi and Banerjee, 1976; King et al., 1983; Tauxe, 1993). Normalization is generally carried out by using a rock magnetic parameter such as anhysteretic remanent magnetization (ARM), isothermal remanent magnetization (IRM), or magnetic susceptibility (κ) to compensate for changes in magnetic concentration of remanence carrying grains. In the last few decades, many RPI records with variable resolution have been obtained from marine sedimentary sequences covering portions of the last several million years (e.g. Valet and Meynadier, 1993; Tauxe and Shackleton, 1994; Channell et al., 1997; Guyodo et al., 2001; Stoner et al., 2003; Thouveny et al., 2004). Reliability of these normalized remanence records as RPI records comes from the observed similarities among RPI records from contrasting environments in the world's oceans (e.g. Guyodo and Valet, 1996, 1999; Laj et al., 2000; Stoner et al., 2002; Yamazaki and Oda, 2005; Channell et al., in press), as well as from the similarity of marine RPI records with lacustrine records (Peck et al., 1996) and with records obtained from marine magnetic anomalies recorded at fast spreading centers (Gee et al., 2000). In addition, the adequate match with cosmogenic isotope records from ice cores over the last ~100 kyr (e.g. Finkel et al., 1997; Baumgartner et al., 1998; Wagner et al., 2000; Muscheler et al., 2005) or sedimentary cores over the last several hundred kyrs (Frank et al., 1997; Carcaillet et al., 2004) indicates that RPI records offer a proxy record of the strength of the main dipole field over these intervals. RPI records not only refine our understanding of temporal geomagnetic field variations and provide data to constrain geodynamo models, they also provide a global stratigraphic tool that augments oxygen isotope records.

Our understanding, however, of the processes responsible for the magnetization of sediments is far from being complete. In addition to field strength, depositional remanence (DRM) is related to mineralogy, concentration and grain size of the magnetic phases, properties of the non-magnetic matrix, and pore water chemistry (Tauxe, 1993). The physical theory concerning particle alignment and magnetization lock-in depends on sediment characteristics that are poorly constrained such as grain flocculation and alignment efficiency (see, e.g. Tauxe et al., 2006). It has long been realized that rock magnetic and other lithological variations induced by paleoclimatic changes can significantly affect or control the NRM, and hence bias RPI records (Kent, 1982). Franke et al. (2004) used a three-member regression model to demonstrate that non-magnetic matrix effects such as opal content, terrigenous content and kaolinite/illite ratio influence RPI records from the South Atlantic.

Attempts have been made to reduce environmental influence on the RPI records by adding, or subtracting a fraction of the normalizer (κ, ARM, or IRM) to/from the normalized intensity record so that the coherence between paleointensity records and their normalizers is minimized. Using this method, the correlation between the paleointensity records obtained with the different normalizers was improved (Mazaud, 2006). A correction function based on the linear relationship between the normalized intensity and the median destructive field of the NRM (considered as grain size proxy) was used by Brachfeld and Banerjee (2000) to reduce the grain size dependence in the RPI records.

2. The recognition and interpretation of orbital cycles in RPI records

Orbital cycles (with ~43 kyr period) were found in the normalized intensity record of the Brunhes Chron from a deep-sea sediment piston core by Kent and Opdyke (1977) using power spectrum analysis, and were interpreted as evidence for orbital forcing on the geodynamo. In recent years, orbital cycles (with ~100 kyr and/or ~41 kyr periods) have also been detected in a number of high-resolution sedimentary relative paleointensity (RPI) records using power spectra (e.g. Channell et al., 1998; Yamazaki, 1999; Thouveny et al., 2004; Yamazaki and Oda, 2005) and wavelet spectra (e.g. Guyodo et al., 2000; Yokoyama and Yamazaki, 2000), as well as in the inclination record using power spectra (Yamazaki and Oda, 2002), and have often been attributed to orbital control on the geodynamo. An orbital cycle with ~100 kyr period was also reported in a ~300 kyr long $^{10}Be/^{9}Be$ record, considered to be a proxy for geomagnetic field strength, from the Portuguese margin (Carcaillet et al., 2004). From three different areas of the Pacific Ocean, Yokoyama et al. (2007) studied the correlations (in terms of correlation coefficients for the entire duration of the records) among the 100-kyr period components extracted from the wavelet transforms of RPI records and rock magnetic parameters. The authors found that RPI variations in the three cores exhibit significant correlation (a single value, 0.55, was used as the threshold for determining the significance of the correlation coefficients), while rock magnetic parameters do not. Therefore, the authors attributed the 100-kyr period in RPI to orbital forcing on the geodynamo.

Orbital periods reported in RPI records have also been attributed to lithologic/climatic contamination. Kok (1999) found that relative paleointensity stacks derived from both normalized NRM (Guyodo and Valet, 1996) and ^{10}Be records (Frank et al., 1997) show coherent features with the oxygen isotope records, and suggested that agreement of the two stacked paleointensity records may stem from similar influences of climate variation rather than from geomagnetic intensity variations alone. Wavelet analyses in the 0–1.1 Ma interval in paleomagnetic records from ODP Site 983 indicated that orbital periods are present in the normalizer records over the same time intervals as in the RPI record, implying that orbital periods embedded in the RPI record are due to the influence of lithologic variations (Guyodo et al., 2000). Roberts et al. (2003) showed that the 100-kyr signal observed by Yamazaki and Oda (2002) in the inclination record from Core MD982185 from the western Caroline Basin is not statistically significant for the entire record, and is not modulated by the 404-ky eccentricity component as might be expected if the inclination record was influenced by orbital eccentricity. Furthermore, based on their coherence analysis (in the frequency domain), highly variable phase relationships and no statistically significant coherence were observed between the

Table 1
Location, water depth, length, sedimentation rate, normalizer, and estimated age for relative paleointensity records used in this study

Records	Location	Water depth (m)	Record length (m)	Sedimentation rate (cm/kyr)	Normalizer used	Oldest age (Ma)	References
ODP 983	60.40N, 23.64W	1983	260	14.7 (2.9–34.6)	ARM, IRM	1.9	Channell et al. (1997, 1998, 2002), Channell and Kleiven (2000)
ODP 984	61.48N, 24.18W	1660	260	13.3 (2.7–41.2)	ARM, IRM	2.15	Channell et al. (1998, 2002), Channell (1999)
ODP 919	62.67N, 37.46W	2088	70	15.6 (7–28)	ARM	0.5	Channell (2006)
IODP U1308	49.87N, 24.23W	3871	85	7.3 (3.8–16)	ARM	1.2	Channell et al. (in press)
ODP 1089	40.94S, 9.89E	4620	88	~17.5 (5–33)	ARM	0.58	Stoner et al. (2003)
MD982185	3.08N, 135.00E	4415	42	~1.5 (1.3–4.9)	ARM	2.25	Yamazaki and Oda (2002, 2005)
MD972143	15.87N, 124.65E	2989	38	~1.5 (0.6–4.6)	Susceptibility	2.14	Horng et al. (2003)

In the sedimentation rate column, mean sedimentation rate is followed by the range of sedimentation rate in parentheses. In the normalizer column, listed are normalizers for RPI data analyzed in this study. Note that for ODP Sites 983 and 984 the normalizer used to generate the RPI records varied downcore, although ARM was generally used. See Fig. 1 for location map of these records.

inclination record and the orbital signal. In addition, Horng et al. (2003) found no orbital cycles in their RPI records from the Western Philippine Sea (Core MD972143) using wavelet methods. No stable orbital periodicities were found in the global RPI stack (SINT800, Guyodo and Valet, 1999), although this could be accounted for by the low time resolution of the stack.

Coherence analysis (in the frequency domain) between the RPI record and the normalizer has been employed (e.g. Tauxe and Wu, 1990; Tauxe, 1993) as a way to determine whether paleointensity records are contaminated by lithologic/climatic factors. The method has been extensively used to assess the quality of individual RPI determinations (e.g. Channell et al., 1998; Channell, 1999; Yamazaki, 1999; Channell and Kleiven, 2000; Yamazaki and Oda, 2005). However, as Valet (2003) pointed out, this type of coherence analysis deals with the entire record and generally does not rule out the possibility that some specific intervals of the two records could exhibit significant coherence on certain frequencies (e.g. orbital frequencies). More sophisticated time-frequency based methods such as cross-wavelet transform and squared wavelet coherence analysis with robust significance tests, has been made available by Torrence and Compo (1998), Torrence and Webster (1999), and by Grinsted et al. (2004). These methods are used by Heslop (2007) to investigate the relationship among orbital, paleoclimatic, and paleointensity changes. The author used the low resolution SINT800 stack (Guyodo and Valet, 1999) and the marine magnetic anomaly paleointensity record of Gee et al. (2000). For these records, it was found that while the paleointensity proxies and orbital variations exhibit common power at certain periods in certain time intervals, they do not exhibit a consistent phase relationship or significant squared wavelet coherence, suggesting no direct physical link between them.

3. Data and methods

In this paper, we use seven previously published high-resolution RPI records from different regions of the world, spanning the past ~2 Myr with good age control, along with rock magnetic records, climate records, and orbital parameters to investigate the origin of orbital periods in these RPI records. The RPI records were first analyzed by local wavelet power spectra (LWPS), with significance tests, to ascertain the presence of orbital periods. Following methods outlined by Torrence and Compo (1998), Torrence and Webster (1999), and by Grinsted et al. (2004), cross-wavelet power spectra (|XWT|), and squared wavelet coherence (WTC), with robust statistical significance tests, were then calculated between RPI records, in which orbital periods exist, and other relevant records such as orbital solutions, benthic oxygen isotope records, normalizer records, grain size proxy records, and physical property records, in order to determine the origin of the orbital periods in the RPI records. Attempts were made to estimate the degree of influence from contamination on the RPI records by comparing RPI records from different regions of the world in both the time domain and time-frequency space after optimally correlating the RPI records to one of the RPI records (ODP Site 984).

Prior to the 1980s, piston cores recovered from the deep sea rarely exceeded a few tens of meters in length (e.g. Kent and Opdyke, 1977). The use of the hydraulic piston corer (HPC) by the Deep Sea Drilling Project (DSDP) and subsequently by the Ocean Drilling Program (ODP), as well as the Calypso coring system of the Marion Dufresne, have revolutionized our ability to collect long relatively undisturbed sediment cores. Sedimentary sequences up to several hundred meters in length can now be recovered by HPC, and this has provided a valuable archive for monitoring detailed changes in the paleomagnetic field. In the last 20 years, many long continuous high-resolution RPI records have become available from the Atlantic (e.g. Channell et al., 1997, in press; Channell, 1999, 2006; Lund et al., 2001a,b; Channell and Raymo, 2003; Stoner et al., 2003), from the equatorial Pacific (e.g. Yamazaki and Oda, 2002; Horng et al., 2003; Yamazaki and Oda, 2005) as well as lower resolution RPI records from North Pacific (Yamazaki, 1999). For this analysis, we have chosen seven high-resolution RPI records with good age control from different regions of the world spanning the past ~2 Ma (Table 1 and Fig. 1). Age models for these records were constructed by correlation of the oxygen isotope records or rock magnetic proxies (e.g. anhysteretic remanent magnetization (ARM), volume susceptibility, or S-ratio) to a reference oxygen isotope curve. Orbital parameters used in this analysis are represented by the ETP curve (Eccentricity + Tilt – Precession) using normalized values from the orbital solutions of Laskar et al. (2004).

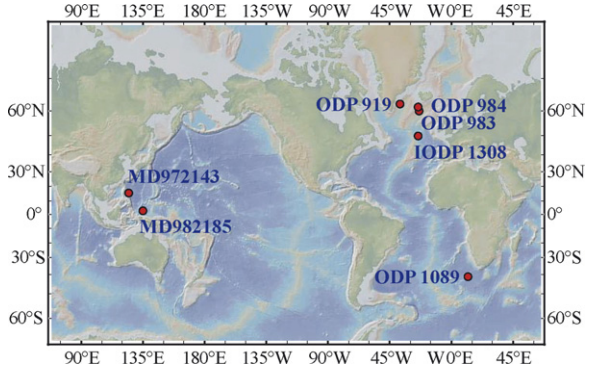

Fig. 1. Location of sites discussed in this study.

The most commonly used way to find frequencies/periods in a time series is power spectrum analysis. The disadvantage of power spectral analysis is that it has only frequency resolution and no time resolution. In addition, it implicitly assumes that the underlying processes are stationary in time, which is generally not true for geophysical processes or their proxy records. In comparison, wavelet transforms expand time series into time frequency space and can therefore detect localized intermittent periodicities, although the spectral estimate with the wavelet method are biased towards the long-wavelength periods (Lau and Weng, 1995; Torrence and Compo, 1998; Grinsted et al., 2004). The Morlet wavelet, a plane wave modulated by a Gaussian envelope, provides a good balance between time and frequency. A Morlet wavelet with a non-dimensional frequency of 6 is used here in our analyses.

Compared with traditional coherence analysis methods (e.g. Tauxe and Wu, 1990; Tauxe, 1993), which reveal phase relationship and coherency between two signals within particular frequency bands (in the frequency domain), cross-wavelet transform and squared wavelet coherence (WTC) are more powerful methods for testing proposed linkages between two time series (Torrence and Compo, 1998; Torrence and Webster, 1999; Grinsted et al., 2004). The cross-wavelet transform reveals common power and relative phase between two time series in the time-frequency domain. For there to be a simple cause and effect relationship between the phenomena recorded in two time series, we would usually expect the oscillations to be phase locked. Squared wavelet coherence can further measure how coherent the cross-wavelet transform is in time-frequency space. The definition of squared wavelet coherence closely resembles that of a traditional correlation coefficient, and it is useful to think of the squared wavelet coherence as a localized correlation coefficient in time frequency space. Compared with Fourier squared coherency, which is used to identify frequency bands within which two time series are co-varying, the squared wavelet coherency is used to identify both frequency bands and time intervals within which the two time series are co-varying (Liu, 1994; Torrence and Webster, 1999).

It is often necessary to address the issue of significance tests for these wavelet-based analyses to distinguish statistically significant results from those due to random chance. Statistical significance of wavelet power can be tested by assuming a χ^2 distribution of the wavelet power spectra and a certain model of the background noise (Torrence and Compo, 1998). For RPI records, a white noise background has been considered to be inadequate (e.g. Barton, 1982; Lund and Keigwin, 1994). Power spectra of RPI records often show continuous power decay with increasing frequency that fit the first order autoregressive AR1 spectrum. Hence, we use AR1 to model the background noise of the RPI data. Using an AR1 noise model, statistical significance levels for the cross-wavelet power can be derived from the square root of the product of two χ^2 distributions, and significance levels of the squared wavelet coherence can be estimated using Monte Carlo methods (Torrence and Webster, 1999; Grinsted et al., 2004).

The records (Table 1) were analyzed using these wavelet-based methods to detect intermittent cyclical behavior in the records, and possibly make connections between RPI records and other records in time-frequency space. As a test of these wavelet methods, LWPS (Fig. 2a and b) of the calculated ETP curve and of the global benthic oxygen isotope stack (LR04 from Lisiecki and Raymo, 2005), and |XWT| (Fig. 2c) and WTC (Fig. 2d) between the two records were performed. Due to the modulating effect of the 404-kyr cycle, eccentricity is only significant (at the 5% significance level) during limited time intervals of the ETP curve (Fig. 2a). LWPS of the

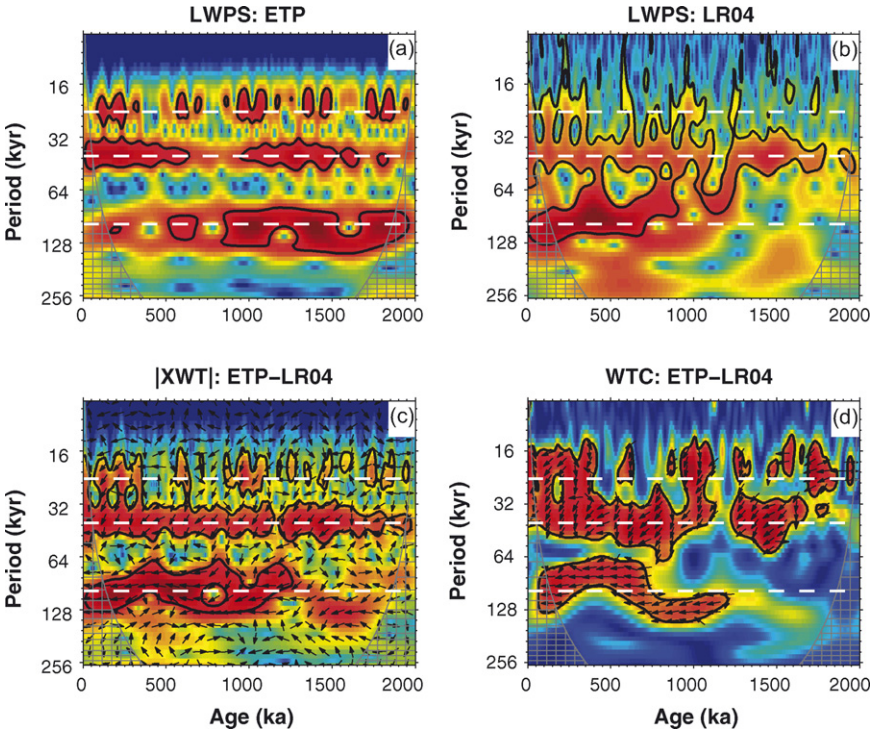

Fig. 2. (a) Local wavelet power spectrum (LWPS) of the ETP curve calculated from normalized value of the Laskar et al. (2004) solution, (b) LWPS of global benthic oxygen isotope stack LR04 from Lisiecki and Raymo (2005), (c) cross-wavelet power spectrum (|XWT|) of the ETP curve and LR04, (d) squared wavelet coherence (WTC) between the ETP curve and LR04. Values of normalized wavelet power, cross-wavelet power, and squared wavelet coherence are indicated using different colors on LWPS, |XWT|, and WTC maps (with blue to red indicating increasing values). The 5% significance level against red noise is shown as thick contours in all figures. The cones of influence (COI) where edge effects make the analyses unreliable are marked by areas of crossed lines. In (c) and (d) the relative phase relationship is shown as arrows (with in-phase pointing right, anti-phase pointing left, and orbital signal leading oxygen isotope signal 90° pointing straight up). Orbital periods of 100 kyr, 41 kyr, and 23 kyr are marked by white dashed lines from bottom to top on the vertical axes.

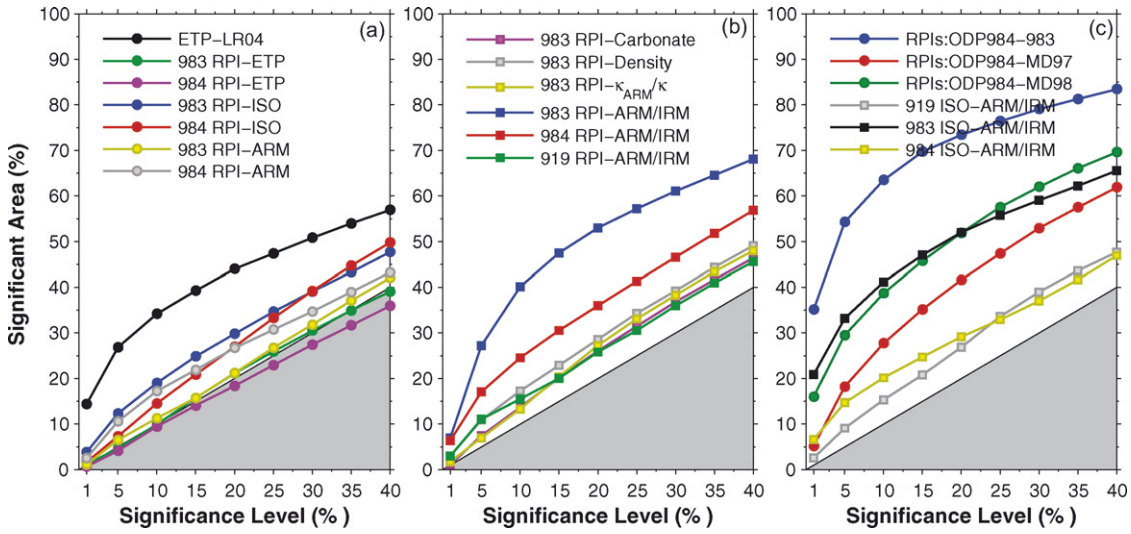

Fig. 3. Percentage of significant area at different significance levels for (a) squared wavelet coherence (WTC) plots in Figs. 2 and 5, (b) WTC plots in Fig. 7a–f, and (c) WTC plots in Figs. 7g–i and Fig. 8. Significance levels of WTC were determined using 500 Monte Carlo runs of randomly generated pairs of red noise that have the same estimated AR1 parameters as the original data. COI was ignored when counting the significant area and the total area on WTC plot. The shaded region indicates results where the percentage of significant area is less than that expected by random chance.

LR04 stack (Fig. 2b) shows the well-known mid-Pleistocene climate transition of significant power from a dominant 41 kyr period to a 100-kyr period at ~800 ka. Since the LR04 stack is a global climate (ice volume) record controlled by orbital forcing, Fig. 2c and d provide a clear demonstration of how the |XWT| and WTC should appear if the two records have a direct physical linkage at particular frequencies/periods. At these frequencies/periods, as expected, we see significant common power on the |XWT| map, significant squared wavelet coherence on the WTC map, and a consistent phase relationship (indicated by arrows on |XWT| and WTC maps) where significant squared wavelet coherence was found (Fig. 2d). Significance levels of all WTC maps in this study were determined using 500 Monte Carlo runs of randomly generated pairs of red noise records that have the same estimated AR1 parameters as the original data. It should be noted that, according to the definition of the significance levels of these wavelet maps, even a purely random time series produces significant peaks above the 5% significance level and makes up 5% of the total area on these wavelet maps (Fig. 4 in Torrence and Compo, 1998). In other words, 5% of all the power on the wavelet maps will exceed that threshold just by chance. To test whether significant areas on WTC maps exceed random levels, we calculated the percentages of significant area at different significance levels for WTC maps, and compiled the results in a figure (Fig. 3) similar to Fig. 5 of Heslop (2007). We ignored data under the cone of influence (COI, region on wavelet maps where edge effects make the analyses unreliable, see caption in Fig. 2) when we count the significant area and the total area on WTC maps. As is shown in Fig. 3a, the percentage of significant area on WTC map between ETP curve and LR04 dramatically exceeds the random levels (shaded regions in Fig. 3) at all significance levels, indicating a link between these two signals.

4. Results and discussion

Local wavelet power spectra with robust significance tests are calculated for the seven RPI records (Table 1) from different regions (Fig. 4). Prior to wavelet analyses, all records have been linearly interpolated into 1-kyr increment time series, linearly detrended, and normalized to have zero mean and unit variance. As can be seen, orbital periods are not significant in RPI records from equatorial Pacific cores MD982185 (Fig. 4f) and MD972143 (Fig. 4g) through time. This result is consistent with analyses by Horng et al. (2003) and Roberts et al. (2003). The variegated character of the LWPS map at periods less than 20 kyr, particularly for Core MD972143 (Fig. 3f), is probably a manifestation of the low resolution (sedimentation rate) of this core. Orbital periods of 100 kyr and/or 41 kyr are significant intermittently in RPI records from North Atlantic (ODP Sites 983, 984, 919, and IODP Site U1308, Fig. 4a–d). For instance, the ~100 kyr period is significant during the ~300–700 ka interval in the ODP Site 983 RPI record (Fig. 4a), and is significant mostly during the ~500–800 ka interval in the ODP Site 984 RPI record (Fig. 4b). The ~100 kyr period is shifted to shorter periods and is limited within the ~550–850 ka time interval in the IODP Site U1308 RPI record (Fig. 4d). Except for the ODP Site 983 RPI record, where it is clearly evident, the ~41 kyr period is significant only intermittently in time frequency space of the other RPI records. For ODP Site 983 RPI record, in which the orbital periods (both 100-kyr and 41-kyr) are most evident, the characteristic mid-Pleistocene climate transition of significant power from a dominant 41-kyr period to a 100-kyr period is observed at ~750 ka (Fig. 4a), probably implying a climatic origin of the orbital periods for this RPI record. In the case of the South Atlantic (ODP Site 1089) RPI record, ~100-kyr periods are significant only in the younger part close to the COI (Fig. 4e). From Fig. 4, we can also see that time intervals where significant power at orbital periods (either 100 kyr or 41 kyr) were detected in the RPI records are not comparable among different RPI records. Although uncertainties in the age models may modulate the wavelet power distribution, they should not be responsible for the absence of orbital periods as long as 41 kyr or 100 kyr. A simple test shows that although the RPI record from equatorial Pacific Core MD972143 shows no significant power at the 100-kyr orbital period (Fig. 4f), LWPS applied to the oxygen isotope record of this core, using the same age model (Horng et al., 2002), clearly shows significant periods of ~100 kyr. Differences in LWPS among these RPI records (Fig. 4) may imply that orbital periods in the RPI records probably do not have a common origin such as direct orbital forcing.

As a further test of whether orbital periods in RPI records are directly due to orbital forcing, |XWT| and WTC between the ETP curve and RPI records from ODP Sites 983 and 984 were calculated (Fig. 5a, d, g and j). Although significant common power was observed at orbital periods between the ETP curve and the RPI records, phase relationships (displayed as arrows on |XWT|

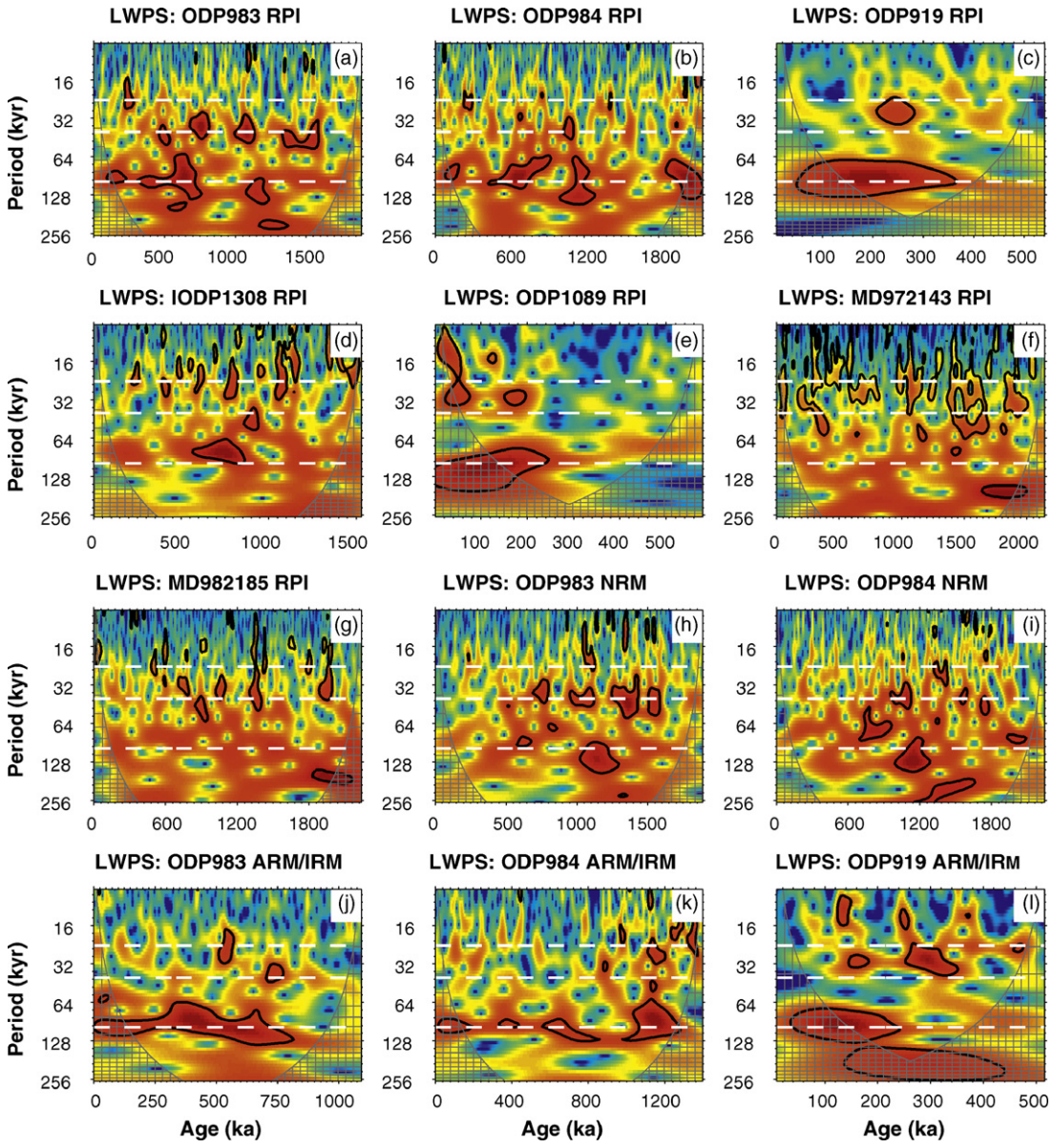

Fig. 4. Local wavelet power spectra (LWPS) of RPI records from (a) Ocean Drilling Program (ODP) Site 983 (Channell et al., 1997, 1998, 2002; Channell and Kleiven, 2000), (b) ODP Site 984 (Channell et al., 1998, 2002; Channell, 1999), (c) ODP Site 919 (Channell, 2006), (d) Integrated Ocean Drilling Program (IODP) Site U1308 (Channell et al., in press), (e) ODP Site 1089 (Stoner et al., 2003), (f) Equatorial Pacific core MD982185 (Yamazaki and Oda, 2002, 2005), (g) Equatorial Pacific core MD972143 (Horng et al., 2003); LWPS of NRM records (from 25 mT demagnetization step) from (h) ODP Site 983 and (i) ODP Site 984; and LWPS of ARM/IRM records from (j) ODP Site 983, (k) ODP Site 984 and (l) ODP Site 919. ARM/IRM records are calculated using ARM and IRM records from 35 mT demagnetization step. See caption of Fig. 2 for description of wavelet maps.

and WTC maps, see caption in Fig. 2 for explanation) between the records vary through time (Fig. 5a and g). The WTC maps (Fig. 5d and j) further suggest that the RPI records are not significantly coherent with the orbital parameters at orbital periods. The percentages of significant areas on these two WTC maps are lower than that generated just by random chance (Fig. 3a). Therefore, orbital periods in RPI records were not caused directly by orbital forcing. It should be noted that wavelet analyses utilized in this study can only reveal the existence of a direct (linear) link between two time series similar to that between the ETP curve and LR04. The possibility of a non-linear relationship between EPT and RPI cannot be excluded. Similarly, |XWT| and WTC were calculated between benthic oxygen isotope records and the RPI records from ODP Sites 983 and 984. The results, however, show significant squared wavelet coherence (Fig. 5e and k) and consistent in-phase relationships along with significant common power at orbital periods between the records (Fig. 5b and h). The percentages of significant area on the WTC maps between RPI records and the oxygen isotope records clearly exceed random levels (Fig. 3a), indicating orbital periods in the RPI records are most likely due to climatic 'contamination'.

To understand the origin of the apparent contamination of RPI records, we test various non-magnetic and magnetic parameters. The first candidate would be the rock magnetic concentration parameters used to normalize the NRM records, for example, anhysteretic remanent magnetization (ARM), isothermal remanent magnetization (IRM), or the susceptibility (κ) record. We test whether orbital periods in RPI records are directly due to the normalizer records. A test for a synthetic RPI record and a synthetic normalizer record show how the |XWT| and WTC map are expected to appear if the orbital periods in RPI records are directly due to

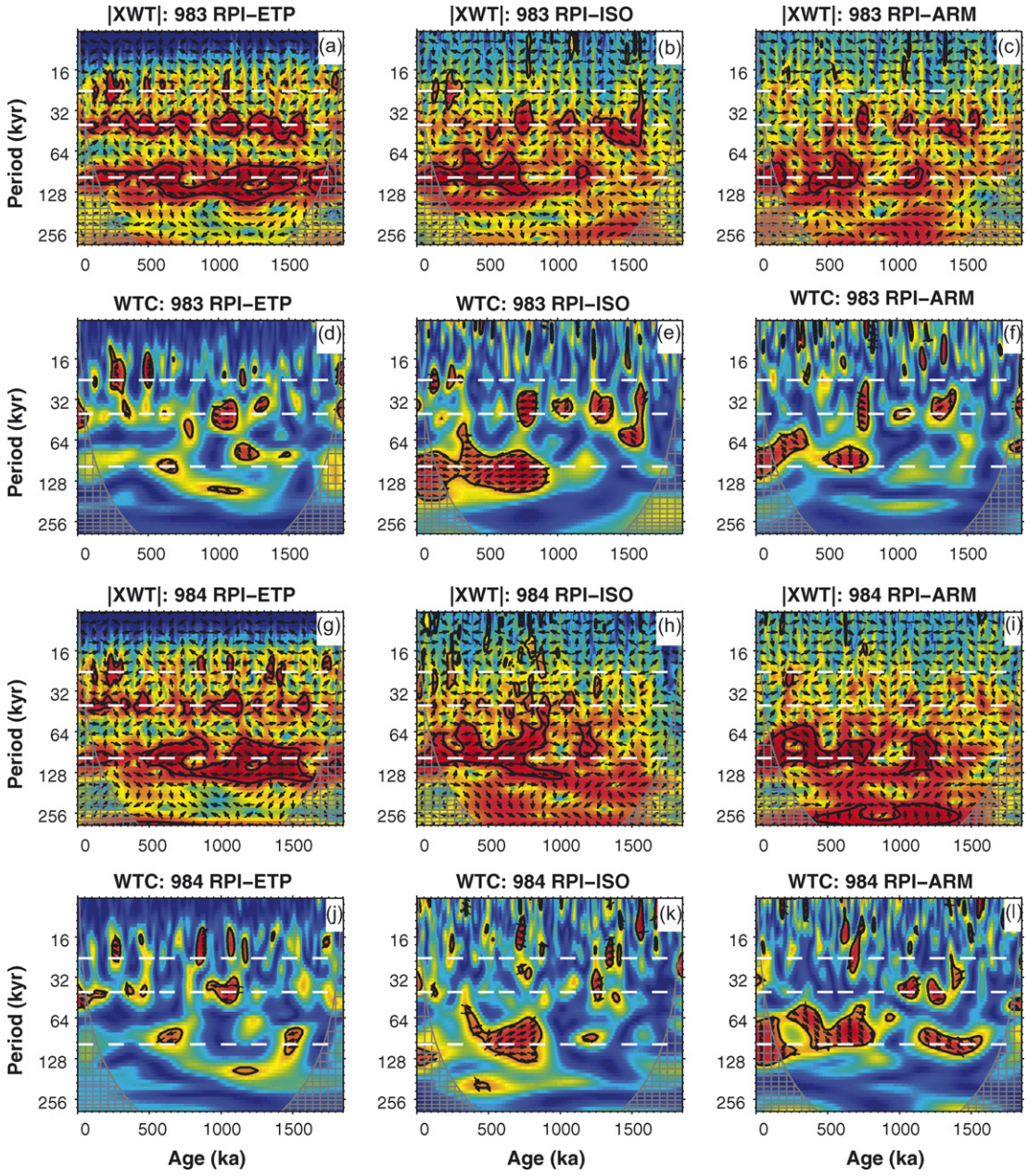

Fig. 5. Cross-wavelet power spectra (|XWT|) of (a) ODP Site 983 RPI record and ETP curve, (b) RPI record and benthic oxygen isotope record from ODP Site 983, (c) RPI record and ARM record from ODP Site 983, (g) ODP Site 984 RPI record and ETP curve, (h) RPI record and benthic oxygen isotope record from ODP Site 984, (i) RPI record and ARM record from ODP Site 984; and squared wavelet coherence (WTC) between (d) ODP Site 983 RPI record and ETP curve, (e) RPI record and benthic oxygen isotope record from ODP Site 983, (f) RPI record and ARM record from ODP Site 983, (j) ODP Site 984 RPI record and ETP curve, (k) RPI record and benthic oxygen isotope record from ODP Site 984, (l) RPI record and ARM record from ODP Site 984. ETP curve was calculated using normalized value of the Laskar et al. (2004) solution. See caption of Fig. 2 for description of wavelet maps, and caption of Fig. 4 for references to ODP Site 983 and 984 data.

the normalizer records (Fig. 6). The synthetic RPI record is calculated using a synthetic NRM record, which is modeled by red noise plus a 100-kyr period during the 500–1000 ka interval, normalized by a synthetic ARM record (normalizer), which includes a 41-kyr period during 500–1000 ka interval, a 100-kyr period during 0–500 ka interval plus a red noise background. The results indicate that orbital periods in the RPI record could come from either the normalizer record (41 kyr period during 500–1000 ka interval, and 100 kyr period during 0–500 ka interval in the synthetic RPI record, see Fig. 6a) or the NRM record (100 kyr period during 500–1000 ka interval in the synthetic RPI record, see Fig. 6a). If the orbital periods in the RPI record are completely and directly due to the normalizer record, we might expect to see consistent phase relationships (anti-phase) and significant squared wavelet coherence (Fig. 6d) along with significant common power (Fig. 6c) between the RPI record and the normalizer record at these orbital periods.

|XWT| and WTC between RPI records and their corresponding normalizer records from ODP Sites 983 and 984 (Fig. 5c, f, I and l) indicate significant common power at orbital periods between RPI records and their normalizers (Fig. 5c and i). The records are significantly coherent (Fig. 5f and l) during certain time intervals, and the percentages of significant area in the WTC maps are also above the random levels (Fig. 3a). However, phase relationships between the RPI records and their normalizer (ARM) records at orbital periods are quite variable (arrows on Fig. 5f and l), implying that 'contamination' (at orbital periods) is not directly or at least not completely

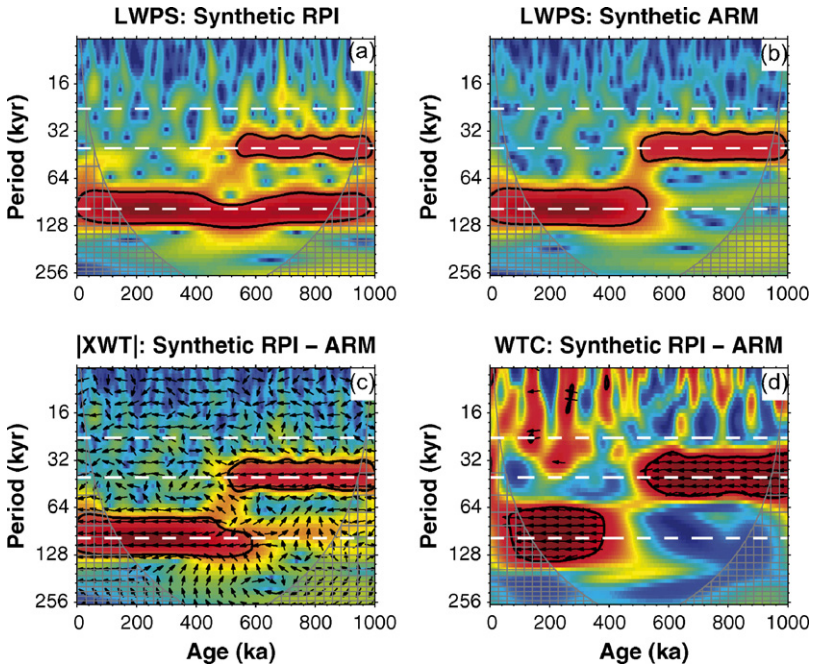

Fig. 6. Local wavelet power spectra (LWPS) of (a) synthetic RPI record and (b) synthetic ARM record, (c) cross-wavelet power spectrum (|XWT|) of the synthetic RPI record and synthetic ARM record, (d) squared wavelet coherence (WTC) between the synthetic RPI record and synthetic ARM record. Synthetic RPI are calculated by normalizing synthetic NRM (modeled using red noise through 0–1000 ka plus a 100-kyr period during 501–1000 ka interval) by a synthetic ARM record (modeled using a 41-kyr period during 501–1000 ka interval and a 100-kyr period during 0–500 ka interval plus red noise background through time). See caption of Fig. 2 for description of wavelet maps.

due to the normalizers. It should be noted that RPI records from ODP Sites 983 and 984 were published in a series of papers (i.e. Channell et al., 1997, 1998, 2002; Channell, 1999; Channell and Kleiven, 2000), and the normalizer used to generate the RPI records varied downcore (Table 1), although ARM was generally used. For these two sites, the two RPI records (normalized using ARM and IRM) are very similar to each other, hence we feel confident using ARM (only) as the normalizer record for the purposes of this test.

Since the NRM record is a combination of geomagnetic field and lithologic variations forced by environment/climate, it is not surprising that orbital periods are significant in the NRM records. This is confirmed by the LWPS of NRM records from ODP Sites 983 (Fig. 4h) and 984 (Fig. 4i). As has been pointed out (e.g. Tauxe et al., 2006), several factors need to be considered when translating DRM into a RPI record: (1) physical theory concerning particle alignment in a viscous medium; (2) compensation for variations in the magnetizability (the choice of normalizer); (3) temporal resolution issues involving the depth at which the magnetization is fixed (lock-in depth) and the degree of smoothing. We ignore the possible influence of temporal resolution issues, and simplify (1) as a parameter called efficiency of alignment which summarizes all factors that may control particle alignment. Further, assuming a uniform magnetic mineralogy (magnetite) in the sediments, normalized intensity record can be expressed as the following equation:

$$\mathrm{RPI} = \frac{\mathrm{NRM}}{\mathrm{ARM}} = \frac{S_{\mathrm{FI}} \times S_{\mathrm{MC}} \times S_{\mathrm{MG}} \times E_{\mathrm{AL}}}{S'_{\mathrm{MC}} \times S'_{\mathrm{MG}}} \quad (1)$$

where NRM represents natural remanent magnetization, ARM represents anhysteretic remanent magnetization, which is the normalizer here, S_{FI} represents magnetic field intensity variation, S_{MC} represents concentration of magnetic minerals (magnetite), S_{MG} represents population of magnetic grains contributing to NRM, E_{AL} represents efficiency of alignment of magnetic grains contributing to NRM, S'_{MC} represents concentration of magnetic minerals (magnetite) contributing to ARM, S'_{MG} represents population of magnetic grains contributing to ARM. We might expect that: $S_{\mathrm{MC}} = S'_{\mathrm{MC}}$, so, we should have:

$$\mathrm{RPI} = \frac{S_{\mathrm{FI}} \times S_{\mathrm{MG}} \times E_{\mathrm{AL}}}{S'_{\mathrm{MG}}} = \left(\frac{S_{\mathrm{MG}}}{S'_{\mathrm{MG}}} \times E_{\mathrm{AL}}\right) \times S_{\mathrm{FI}} \quad (2)$$

Therefore, if there were any 'contamination' in the RPI record, we would expect it to be from the incompletely normalized component: $(S_{\mathrm{MG}}/S'_{\mathrm{MG}}) \times E_{\mathrm{AL}}$. One way to find the origin of the 'contamination' would be by looking at the |XWT| and WTC between the RPI records and other proxy records that may potentially represent the incompletely normalized component, for instance, grain size proxies (may mimic $S_{\mathrm{MG}}/S'_{\mathrm{MG}}$ variation) or physical properties (could influence E_{AL}).

For ODP Site 983, the WTC between the RPI record and physical properties, such as carbonate content and GRA (gamma-ray attenuation) density, and between the RPI record and grain size proxies, such as $\kappa_{\mathrm{ARM}}/\kappa$ (κ_{ARM} is the anhysteretic remanent susceptibility, and κ is the volume susceptibility) and ARM/IRM were calculated (Fig. 7a–d). Although percentages of significant area on the WTC maps between RPI records and physical properties from ODP Site 983 are above the random levels (Fig. 3b), the phase relationships vary through time, 'contamination' in RPI records is hence not directly related to physical properties such as GRA density (Fig. 7b) or carbonate content (Fig. 7a). This indicates that either these physical properties are not good proxies of E_{AL}, or E_{AL} has little contribution to 'contamination'. Similarly, 'contamination' is not directly related to grain size proxy $\kappa_{\mathrm{ARM}}/\kappa$ at ODP Site 983 (Fig. 7c and Fig. 3b). However, significant squared wavelet coherence and a consistent phase relationship (in-phase) at orbital periods between the RPI record and the grain size proxy ARM/IRM (Fig. 7d) indicate that 'contamination' in the RPI record appears to be reflected by ARM/IRM. We further tested the WTC between RPI records and grain size proxy ARM/IRM for ODP Site 984 and ODP Site 919. The results (Fig. 7e and f) are consistent with result for ODP Site 983. Significant squared wavelet coherence and consistent in-phase relationship at orbital periods between RPI record

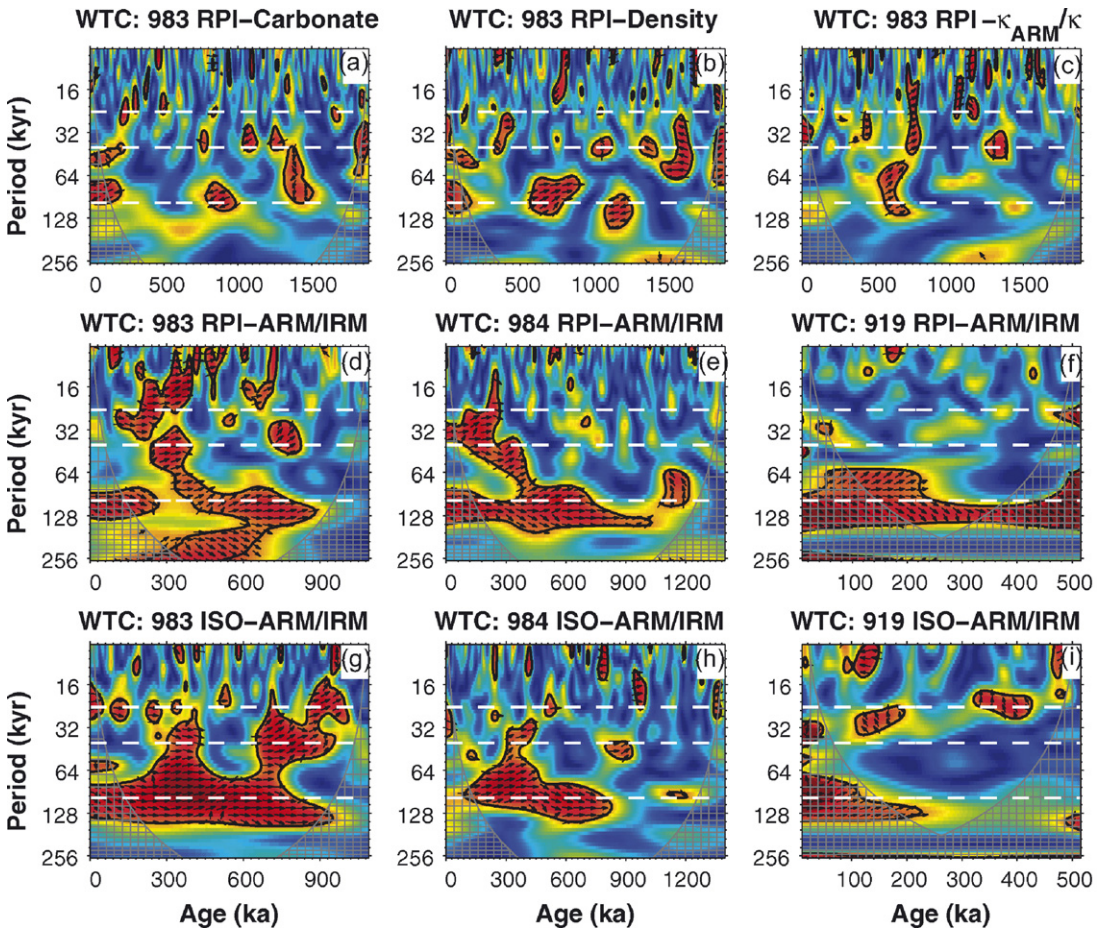

Fig. 7. Squared wavelet coherence (WTC) between (a) RPI record and carbonate content record from ODP Site 983, (b) RPI record and GRA (gamma-ray attenuation) density record from ODP Site 983, (c) RPI record and κ_{ARM}/κ record from ODP Site 983, (d) RPI record and ARM/IRM record from ODP Site 983, (e) RPI record and ARM/IRM record from ODP Site 984, and (f) RPI record and ARM/IRM record from ODP Site 919, (g) benthic oxygen isotope record and ARM/IRM record from ODP Site 983, (h) benthic oxygen isotope record and ARM/IRM record from ODP Site 984, (i) planktic oxygen isotope record and ARM/IRM record from ODP Site 919. ARM/IRM is calculated using ARM and IRM records from 35 mT demagnetization step. See caption of Fig. 2 for description of wavelet maps, and caption of Fig. 4 for references of the paleomagnetic data. Carbonate content data of ODP Site 983 are from Ortiz et al. (1999). GRA density data of ODP Site 983 are from Shipboard Scientific Party (1996).

and grain size proxy ARM/IRM, together with significant common power were observed for records from these two sites. The percentages of significant area on the WTC maps between RPI records and ARM/IRM records from these sites are dramatically above random levels (Fig. 3b).

ARM/IRM ratios are widely employed as grain size indicators for magnetite (e.g. Meynadier et al., 1995; Rousse et al., 2006; Venuti et al., 2007). Because ARM is more effective in activating finer magnetite grains than IRM, small (large) particles lead to higher (lower) values of the ratio. The dependence of various rock magnetic parameters such as κ_{ARM}, SIRM, and κ on magnetite grain size has been studied by many researchers (e.g. Maher, 1988; Dunlop and Argyle, 1997; Dunlop and Özdemir, 1997; Egli and Lowrie, 2002). κ_{ARM}, SIRM, and κ activate different grain size populations. The ARM/IRM ratio depicts the relative population of magnetic grains contributing to ARM to the population of magnetic grains contributing to IRM in the sediments. The ARM/IRM ratio appears to influence the RPI proxies (e.g. NRM/ARM) while the κ_{ARM}/κ ratio may not because κ is sensitive to magnetic grains with much larger grain size that are unlikely to carry appreciable remanence.

Changes in fraction of certain grain sizes (i.e. sortable silt with grain size ranging ~10–63 μm) have been proposed as reliable tracers of the bottom current behavior (McCave et al., 1995). Prins et al. (2002) demonstrated that, for some North Atlantic sites on the Reykjanes Ridge, well-sorted clay to fine silt fractions with a peak distribution <10 μm provide a better proxy for the behavior of bottom currents because of an important silt fraction in ice rafted debris (IRD). Snowball and Moros (2003) analyzed cores that are also from the Reykjanes ridge and noted that the magnetic grain size distribution of the sediments lies within the size range considered by Prins et al. (2002), and hence is suitable for reconstruction of the near-bottom current velocity. Coarse (fine) grains within this grain size fraction would generally imply enhanced (reduced) bottom current strength, presumably related to the formation of North Atlantic deep Water (NADW). As ODP Site 919 (Clausen, 1998), and ODP Sites 983 and 984 (Bianchi and McCave, 2000) are located on the flow path of NADW, it is likely that variations in bottom current behavior at these sites correspond to climatic changes on orbital time scales. Significant power at ~100 kyr period is clearly observed in ARM/IRM records from these sites that is coherent with the oxygen isotope records. See Fig. 4j–l for LWPS of the ARM/IRM record, Fig. 7g–i for WTC maps between the oxygen isotope records and ARM/IRM records, and Fig. 3c for results of testing the significant areas on WTC maps against random chance. Lack of significant WTC between the oxygen isotope and ARM/IRM records from ODP Site 919 (Fig. 7i) may be a reflection of meltwater related perturbations on the planktic oxygen isotope record at this site (St. John et al., 2004). It is likely that orbital periods in the RPI records were introduced into the NRM records (and have not been normalized) through climatic control on bottom current velocity, which in turn

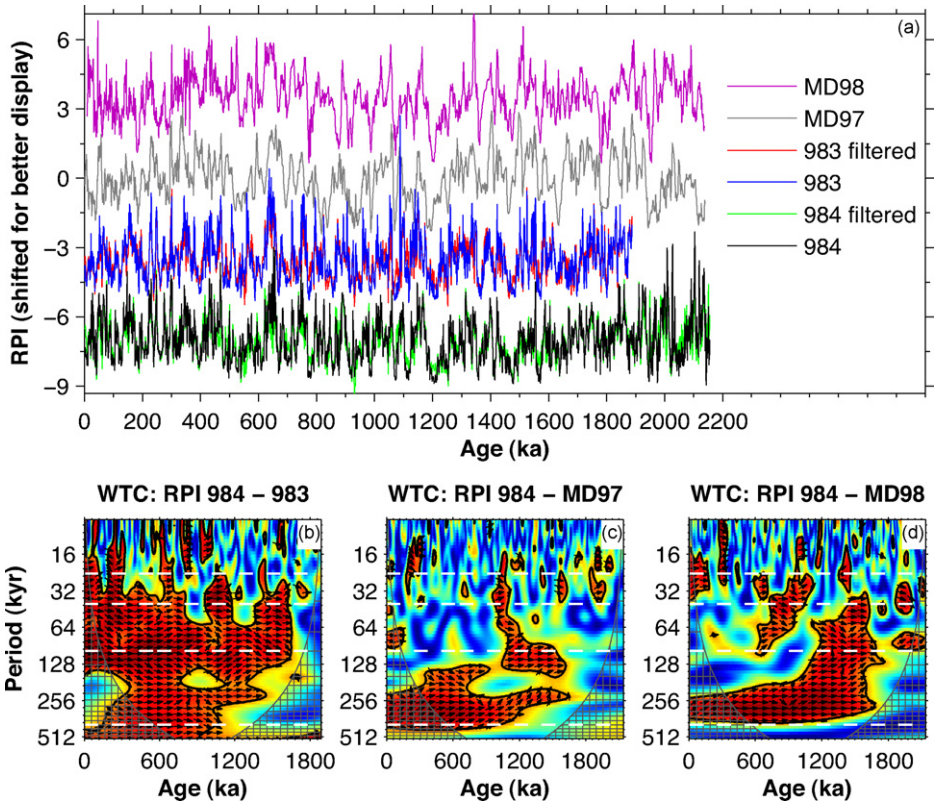

Fig. 8. (a) Comparing RPI records in the time domain: RPI records are from the equatorial Pacific (MD982185 and MD972143) and North Atlantic (ODP Sites 983 and 984), also shown are RPI records of ODP Sites 983 and 984 with orbital periods filtered (bandstop filtering was applied with stop bands located at (1/120) ~ (1/80) kyr^{-1} frequencies and at (1/50) ~ (1/30) kyr^{-1} frequencies). Comparing RPI records in the time frequency domain: (b) WTC between RPI records from ODP Sites 984 and 983, (c) WTC between RPI records from ODP Site 984 and equatorial Pacific Core MD972143, and (d) WTC between RPI records from ODP Site 984 and equatorial Pacific Core MD982185. To reduce discrepancies from age models, RPI records have been first optimally correlated to ODP Site 984 RPI record using the "Match" protocol of Lisiecki and Lisiecki (2002). In (a) RPI scale has been shifted for each record for better display. See caption of Fig. 2 for description of the WTC maps, and caption in Fig. 4 for references for the RPI records. The additional dashed white lines on the bottom of (b), (c), and (d) mark the 404-kyr period on the vertical axes.

controls the magnetic grain size distribution (corresponds to the S_{MG}/S'_{MG} component in Eq. (2)) of the sediments. Changes in bottom current velocity in the North Atlantic are accompanied by variation in grain size and concentration of magnetic parameters (e.g. Kissel et al., 1999; Ballini et al., 2006). As floc size is controlled by shear stress (current velocity) and particle concentration (Winterwerp and Kesteren, 2004), changes in bottom current velocity at orbital periods may introduce additional effects on the NRM record that amplify the contamination at orbital periods (in terms of efficiency of alignment, E_{AL} in Eq. (2)).

Since 'contamination' exists in the RPI records, one critical question is whether the 'contamination' is debilitating to the RPI records as a geomagnetic signal, and as a useful stratigraphic correlation tool. First of all, as can be seen from WTC between RPI records and benthic oxygen isotope records from ODP Sites 983 and 984 (Fig. 5e and k), climatic 'contamination' (area with significant common power, consistent in-phase relationship, and significant squared wavelet coherence on |XWT| and WTC maps) exists only at orbital periods during some time intervals. Secondly, a comparison was made between RPI records from different regions of the world (ODP Sites 983 and 984 from North Atlantic, and cores MD972143 and MD982185 from equatorial Pacific). It appears that these RPI records are highly comparable with each other in the time domain (Fig. 8a). To reduce discrepancies attributable to age models, RPI records have been first optimally correlated to the ODP Site 984 RPI record using the "Match" protocol of Lisiecki and Lisiecki (2002). We also compared the RPI records from ODP Sites 983 and 984 before and after filtering the orbital periods from the RPI records. A bandstop filter has been applied to the RPI records with stop bands located at (1/120) ~ (1/80) kyr^{-1} frequencies and at (1/50) ~ (1/30) kyr^{-1} frequencies. It appears that filtering does not alter the RPI records very much (Fig. 8a). This is not surprising when we look at the WTC maps of these RPI records (Fig. 8b–d, also see Fig. 3c for significance tests for the WTC maps). The 'common' features (indicated by significant WTC values and in-phase relationship) in these RPI records span a large range of periods (~16–400 kyr). These results suggest that 'contamination', although it exists in the RPI records (at orbital periods), does not strongly affect the characteristic features of the paleointensity records, and hence is not debilitating to these RPI records as a global signal that is primarily of geomagnetic origin.

5. Conclusions

The present study confirms previous analyses that orbital periods are not significant in RPI records from equatorial Pacific cores MD982185 and MD972143 through time. Orbital periods are significant only during limited time intervals in RPI records from North Atlantic (ODP Sites 919, 983, 984, IODP Site U1308), and South Atlantic (ODP Site 1089). The characteristic mid-Pleistocene climate transition is observed in the ODP Site 983 RPI record, in which the orbital periods are most evident, indicating a possible climatic origin of the orbital periods for this RPI record. The fact that time intervals where orbital periods are significant are not comparable among RPI records from different regions provides evidence that orbital periods in the RPI records are not directly due to orbital forcing. This is further indicated by the |XWT| and WTC between ETP curve and RPI records from ODP Sites 983 and 984. The |XWT| and

WTC between benthic oxygen isotope records and the RPI records from ODP Sites 983 and 984, however, show significant coherence and consistent in-phase relationships at orbital periods and hence imply that orbital periods in the RPI records are most likely due to climatic 'contamination'.

Phase relationships between RPI records and their corresponding normalizer records from ODP Sites 983 and 984 exclude the possibility that 'contamination' (at orbital periods) is directly or completely due to the normalizers. As suggested by the analysis of a synthetic RPI record and a synthetic normalizer record, we may expect to see consistent anti-phase relationship along with significant squared wavelet coherence between RPI and the normalizer if orbital periods in the RPI record are completely and directly due to the normalizer record. Orbital periods are significant in the NRM records from ODP Sites 983 and 984. Deduction from the theoretical RPI model attributes the 'contamination' in RPI records to incompletely normalized component of the NRM records. Further tests of records from ODP Site 983 indicate that 'contamination' is apparently not directly related to physical properties such as density or carbonate content, and the grain size proxy κ_{ARM}/κ. WTC between RPI records and grain size proxy ARM/IRM from ODP Sites 919, 983, and 984 imply that ARM/IRM may mimic the 'contamination' in the RPI records at these sites. Orbital periods were probably introduced into the NRM records (and have not been normalized when calculating RPI records) through orbital control on the bottom current velocity that regulated NADW formation, which in turn controls magnetic grain size distribution at the site, and possibly also the degree of particle flocculation.

Four lines of evidence indicate that 'contamination', although it exists in these RPI records, is not debilitating to these RPI records as a global signal that is primarily of geomagnetic origin: (1) 'contamination' exists only at orbital periods during limited time intervals. (2) RPI records from different regions of the world (ODP Sites 983 and 984 from North Atlantic, and cores MD972143 and MD982185 from equatorial Pacific) are highly comparable with each other in the time domain. In view of the contrasting climatic/lithologic characteristics of the North Atlantic and equatorial Pacific, we would not expect to observe this level of similarity if the RPI records were dominated by lithologic contamination. (3) Filtering orbital periods from the RPI records does not alter the RPI records appreciably other than reducing the amplitude of certain features in the records. (4) WTCs among these RPI records show large areas (spanning a large range of periods: ~16–400 kyr) characterized by significant coherence and in-phase relationships.

Acknowledgements

This paper was presented at the International Symposium on "Paleomagnetism and the Earth's Deep Interior: Unsolved Problems and Future Challenges" in Beijing in July 2007. The authors thank T. Yamazaki and C.-S. Horng for providing the paleomagnetic data of Cores MD982185 and MD972143, respectively, from the equatorial Pacific. The authors also thank M. Winklhofer and the other journal reviewer for comments that improved the manuscript. Wavelet analyses were performed using a modified versions of MATLAB code originally written by C. Torrence and G. Compo, and by A. Grinsted. This study was supported by NSF grant OCE-0350830.

References

Ballini, M., Kissel, C., Colin, C., Richter, T., 2006. Deep-water mass source and dynamic associated with rapid climatic variations during the last glacial stage in the North Atlantic: a multiproxy investigation of the detrital fraction of deep-sea sediments. Geochem. Geophys. Geosyst. 7, Q02N01, doi:10.1029/2005GC001070.

Barton, C.E., 1982. Spectral-analysis of paleomagnetic time-series and the geomagnetic spectrum. Philos. Trans. R. Soc. Lond. A 306, 203–209.

Baumgartner, S., Beer, J., Masarik, J., Wagner, G., Meynadier, L., Synal, H.A., 1998. Geomagnetic modulation of the ^{36}Cl flux in the GRIP ice core, Greenland. Science 279, 1330–1332.

Bianchi, G.G., McCave, I.N., 2000. Hydrography and sedimentation under the deep western boundary current on Bjorn and Gardar Drifts. Iceland Basin Mar. Geol. 165, 137–169.

Brachfeld, S.A., Banerjee, S.K., 2000. A new high-resolution geomagnetic relative paleointensity record for the North American Holocene: a comparison of sedimentary and absolute intensity data. J. Geophys. Res. 105, 821–834.

Bullard, E.C., 1949. The magnetic field within the Earth. Proc. R. Soc. Lond., Ser. A 197, 433–453.

Carcaillet, J., Bourles, D.L., Thouveny, N., Arnold, M., 2004. A high resolution authigenic ^{10}Be/^{9}Be record of geomagnetic moment variations over the last 300 ka from sedimentary cores of the Portuguese margin. Earth Planet. Sci. Lett. 219, 397–412.

Channell, J.E.T., 1999. Geomagnetic paleointensity and directional secular variation at Ocean Drilling Program (ODP) Site 984 (Bjorn Drift) since 500 ka: comparisons with ODP Site 983 (Gardar Drift). J. Geophys. Res. 104 (22), 937-22,951.

Channell, J.E.T., 2006. Late Brunhes polarity excursions (Mono Lake, Laschamp, Iceland Basin and Pringle Falls) recorded at ODP Site 919 (Irminger Basin). Earth Planet. Sci. Lett. 244, 378–393.

Channell, J.E.T., Hodell, D.A., Lehman, B., 1997. Relative geomagnetic paleointensity and δ^{18}O at ODP Site 983 (Gardar Drift, North Atlantic) since 350 ka. Earth Planet. Sci. Lett. 153, 103–118.

Channell, J.E.T., Hodell, D.A., McManus, J., Lehman, B., 1998. Orbital modulation of the Earth's magnetic field intensity. Nature 394, 464–468.

Channell, J.E.T., Mazaud, A., Sullivan, P., Turner, S., Raymo, M.E., 2002. Geomagnetic excursions and paleointensities in the Matuyama Chron at Ocean Drilling Program Sites 983 and 984 (Iceland Basin). J. Geophys. Res. 107, 2114, doi:10.1029/2001JB000491.

Channell, J.E.T., Hodell, D.A., Xuan, C., Mazaud, A., Stoner, J.S., in press. A calibrated 1.5 Myr record of relative paleointensity from IODP Site U1308 (North Atlantic). Earth Planet. Sci. Lett.

Channell, J.E.T., Kleiven, H.F., 2000. Geomagnetic palaeointensities and astrochronological ages for the Matuyama–Brunhes boundary and the boundaries of the Jaramillo Subchron: palaeomagnetic and oxygen isotope records from ODP Site 983. Philos. Trans. R. Soc. Lond. A 358, 1027–1047.

Channell, J.E.T., Raymo, M.E., 2003. Paleomagnetic record at ODP Site 980 (Feni Drift Rockall) for the past 1.2 Myrs. Geochem. Geophys. Geosyst. 4, 1033, doi:10.1029/2002GC000440.

Christensen, U.R., Tilgner, A., 2004. Power requirement of the geodynamo from ohmic losses in numerical and laboratory dynamos. Nature 429, 169–171.

Clausen, L., 1998. Late Neogene and Quaternary sedimentation on the continental slope and upper rise offshore southeast Greenland: interplay of contour and turbidity processes. In: Larsen, H.C., Saunders, A.D., Wise Jr., S.W. (Eds.), Proc. ODP, Sci. Results, 152. Ocean Drilling Program, College Station, TX, pp. 3–18.

Dunlop, D.J., Argyle, K.S., 1997. Thermoremanence anhysteretic remanence and susceptibility of submicron magnetites: nonlinear field dependence and variation with grain size. J. Geophys. Res. 102 (20), 199-20,210.

Dunlop, D.J., Özdemir, Ö., 1997. Rock Magnetism: Fundamentals and Frontiers. Cambridge University Press, New York, pp. 573.

Egli, R., Lowrie, W., 2002. Anhysteretic remanent magnetization of fine magnetic particles. J. Geophys. Res. 107, 2209, doi:10.1029/2001JB000671.

Finkel, R.C., Nishiizumi, K., Hammer, C.U., Mayewski, P.A., Peel, D., Stuiver, M., 1997. Beryllium 10 concentrations in the Greenland Ice Sheet Project 2 ice core from 3–40 ka. J. Geophys. Res. 102 (26), 699-26,706.

Frank, M., Schwarz, B., Baumann, S., Kubik, P.W., Suter, M., Mangini, A., 1997. A 200 kyr record of cosmogenic radionuclide production rate and geomagnetic field intensity from Be-10 in globally stacked deep-sea sediments. Earth Planet. Sci. Lett. 149, 121–129.

Franke, C., Hofmann, D., von Dobeneck, T., 2004. Does lithology influence relative paleointensity records: a statistical analysis on South Atlantic pelagic sediments. Phys. Earth Planet. Inter. 147, 285–296.

Fuller, M., 2006. Geomagnetic field intensity, excursions, reversals and the 41,000-yr obliquity signal. Earth Planet. Sci. Lett. 245, 605–615.

Gee, J.S., Cande, S.C., Hildebrand, J.A., Donnelly, K., Parker, R.L., 2000. Geomagnetic intensity variations over the past 780 kyr obtained from near-seafloor magnetic anomalies. Nature 408, 827–832.

Glatzmaier, G.A., Coe, R.S., Hongre, L., Roberts, P.H., 1999. The role of the Earth's mantle in controlling the frequency of geomagnetic reversals. Nature 401, 885–890.

Glatzmaier, G.A., Roberts, P.H., 1996. Rotation and magnetism of Earth's inner core. Science 274, 1887–1891.

Grinsted, A., Moore, J.C., Jevrejeva, S., 2004. Application of the cross wavelet transform and wavelet coherence to geophysical time series. Nonlin. Process. Geophys. 11, 561–566.

Gubbins, D., Roberts, P.H., 1987. Magnetohydrodynamics of the Earth's core. In: Jacobs, J. (Ed.), Geomagnetism. Academic Press, London, pp. 1–183.

Guyodo, Y., Acton, G.D., Brachfeld, S., Channell, J.E.T., 2001. A sedimentary paleomagnetic record of the Matuyama Chron from the western Antarctic margin (ODP Site 1101). Earth Planet. Sci. Lett. 191, 61–74.

Guyodo, Y., Gaillot, P., Channell, J.E.T., 2000. Wavelet analysis of relative geomagnetic paleointensity at ODP Site 983. Earth Planet. Sci. Lett. 184, 109–123.

Guyodo, Y., Valet, J.-P., 1999. Global changes in intensity in the Earth's magnetic field during the past 800 kyr. Nature 399, 249–252.

Guyodo, Y., Valet, J.P., 1996. Relative variations in geomagnetic intensity from sedimentary records: the past 200,000 years. Earth Planet. Sci. Lett. 143, 23–36.
Heslop, D., 2007. A wavelet investigation of possible orbital influences on past geomagnetic field intensity. Geochem. Geophys. Geosyst. 8, Q03003, doi:10.1029/2006GC001498.
Horng, C.-S., Roberts, A.P., Liang, W.-T., 2003. A 2.14-Myr astronomically tuned record of relative geomagnetic paleointensity from the western Philippine Sea. J. Geophys. Res. 108, 2059, doi:10.1029/2001JB001698.
Horng, C.S., Lee, M.Y., Palike, H., Wei, K.Y., Liang, W.T., 2002. Astronomically calibrated ages for geomagnetic reversals within the Matuyama chron. Earth Planets Space 54, 679–690.
Johnson, E.A., Murphy, T., Torreson, O.W., 1948. Prehistory of the Earth's magnetic field. J. Geophys. Res. 53, 349–372.
Kent, D.V., 1982. Apparent correlation of palaeomagnetic intensity and climatic records in deep-sea sediments. Nature 299, 538–539.
Kent, D.V., Carlut, J., 2001. A negative test of orbital control of geomagnetic reversals and excursions. Geophys. Res. Lett. 28, 3561–3564.
Kent, D.V., Opdyke, N.D., 1977. Paleomagnetic field intensity variation recorded in a Brunhes epoch deep-sea sediment core. Nature 266, 156–159.
Kerswell, R.R., 1996. Upper bounds on the energy dissipation in turbulent precession. J. Fluid Mech. 321, 335–370.
King, J.W., Banerjee, S.K., Marvin, J., 1983. A new rock-magnetic approach to selecting sediments for geomagnetic paleointensity studies; application to paleointensity for the last 4000 years. J. Geophys. Res. 88, 5911–5921.
Kissel, C., Laj, C., Labeyrie, L., Dokken, T., Voelker, A., Blamart, D., 1999. Rapid climatic variations during marine isotopic stage 3: magnetic analysis of sediments from Nordic Seas and North Atlantic. Earth Planet. Sci. Lett. 171, 489–502.
Kok, Y.S., 1999. Climatic influence in NRM and 10Be-derived geomagnetic paleointensity data. Earth Planet. Sci. Lett. 166, 105–119.
Laj, C., Kissel, C., Mazaud, A., Channell, J.E.T., Beer, J., 2000. North Atlantic palaeointensity stack since 75 ka (NAPIS-75) and the duration of the Laschamp event. Philos. Trans. R. Soc. Lond. A 358, 1009–1025.
Laskar, J., Robutel, P., Joutel, F., Gastineau, M., Correia, A.C.M., Levrard, B., 2004. A long-term numerical solution for the insolation quantities of the Earth. Astron. Astrophys. 428, 261–285.
Lau, K.M., Weng, H., 1995. Climate signal detection using wavelet transform: how to make a time series sing. Bull. Am. Meteor. Soc. 76, 2391–2402.
Levi, S., Banerjee, S.K., 1976. On the possibility of obtaining relative paleointensities from lake sediments. Earth Planet. Sci. Lett. 29, 219–226.
Lisiecki, L.E., Lisiecki, P.A., 2002. Application of dynamic programming to the correlation of paleoclimate records. Paleoceanography 17, 1049, doi:10.1029/2001PA000733.
Lisiecki, L.E., Raymo, M.E., 2005. A Pliocene–Pleistocene stack of 57 globally distributed benthic δ18O records. Paleoceanography 20, PA1003, doi:10.1029/2004PA001071.
Liu, P.C., 1994. Wavelet spectrum analysis and ocean wind waves. In: Foufoula-Georgiou, E., Kumar, P. (Eds.), Wavelets in Geophysics. Academic Press, New York, pp. 151–166.
Loper, D.E., 1975. Torque balance and energy budget for the precessionally driven dynamo. Phys. Earth Planet. Inter. 11, 43–60.
Lund, S.P., Acton, G.D., Clement, B.M., Okada, M., Williams, T., 2001a. Paleomagnetic records of Stage 3 excursions. Leg 172. In: Keigwin, L.D., Rio, D., Acton, G.D., Arnold, E. (Eds.), Proc. ODP, Sci. Results, 172. Ocean Drilling Program, College Station, TX, pp. 1–20.
Lund, S.P., Keigwin, L., 1994. Measurement of the degree of smoothing in sediment paleomagnetic secular variation records—an example from late Quaternary deep-sea sediments of the Bermuda rise, western North-Atlantic Ocean. Earth Planet. Sci. Lett. 122, 317–330.
Lund, S.P., Williams, T., Acton, G.D., Clement, B.M., Okada, M., 2001b. Brunhes Chron magnetic field excursions recovered from Leg 172 sediments. In: Keigwin, L.D., Rio, D., Acton, G.D., Arnold, E. (Eds.), Proc. ODP, Sci. Results, 172. Ocean Drilling Program, College Station, TX, pp. 1–18.
Maher, B.A., 1988. Magnetic-properties of some synthetic sub-micron magnetites. Geophys. J. Int. 94, 83–96.
Malkus, W.V.R., 1968. Precession of the Earth as the cause of geomagnetism. Science 160, 259–264.
Mazaud, A., 2006. A first-order correction to minimize environmental influence in sedimentary records of relative paleointensity of the geomagnetic field. Geochem. Geophys. Geosyst. 7, Q07002, doi:10.1029/2006GC001257.
McCave, I.N., Manighetti, B., Robinson, S.G., 1995. Sortable silt and fine sediment size composition slicing—parameters for paleocurrent speed and paleoceanography. Paleoceanography 10, 593–610.
Meynadier, L., Valet, J.P., Grousset, F.E., 1995. Magnetic-properties and origin of upper Quaternary sediments in the Somali basin. Indian-Ocean. Paleoceanography 10, 459–472.
Muscheler, R., Beer, R., Kubik, P.W., Synal, H.A., 2005. Geomagnetic field intensity during the last 60,000 years based on Be-10 and Cl-36 from the Summit ice cores and C-14. Quat. Sci. Rev. 24, 1849–1860.
Ortiz, J., Mix, A., Harris, S., O'Connell, S., 1999. Diffuse spectral reflectance as a proxy for percent carbonate contnet in north Atlantic sediments. Paleoceanography 14, 171–186.
Peck, J.A., King, J.W., Colman, S.M., Kravchinsky, V.A., 1996. An 84-kyr paleomagnetic record from the sediments of Lake Baikal, Siberia. J. Geophys. Res. 101, 11365–11385.
Prins, M.A., Bouwer, L.M., Beets, C.J., Troelstra, S.R., Weltje, G.J., Kruk, R.W., Kuijpers, A., Vroon, P.Z., 2002. Ocean circulation and iceberg discharge in the glacial North Atlantic: inferences from unmixing of sediment size distributions. Geology 30, 555–558.
Roberts, A.P., Winklhofer, M., Liang, W.-T., Horng, C.-S., 2003. Testing the hypothesis of orbital (eccentricity) influence on Earth's magnetic field. Earth Planet. Sci. Lett. 216, 187–192.
Rochester, M.G., Jacobs, J.A., Smylie, D.E., Chong, K.F., 1975. Can precession power the geomagnetic dynamo? Geophys J. R. Astron. Soc. 43, 661–678.
Rousse, S., Kissel, C., Laj, C., Eiriksson, J., Knudsen, K.L., 2006. Holocene centennial to millennial-scale climatic variability: evidence from high-resolution magnetic analyses of the last 10 cal kyr off North Iceland (core MD99-2275). Earth Planet. Sci. Lett. 242, 390–405.
Shipboard Scientific Party, 1996. Site 983. In: Jansen, E., M. Raymo, P. Blum, et al. (eds.), Proc. ODP, Init. Repts., 162. Ocean Drilling Program, College Station, TX, pp. 139–167.
Snowball, I., Moros, M., 2003. Saw-tooth pattern of North Atlantic current speed during Dansgaard–Oeschger cycles revealed by the magnetic grain size of Reykjanes Ridge sediments at 59 degrees N. Paleoceanography 18, 1026, doi:10.1029/2001PA000732.
St. John, K., Flower, B.P., Krissek, L., 2004. Evolution of iceberg melting, biological productivity, and the record of Icelandic volcanism in the Irminger basin since 630 ka. Mar. Geol. 212, 133–152.
Stoner, J.S., Channell, J.E.T., Hodell, D.A., Charles, C.D., 2003. A ~580 kyr paleomagnetic record from the sub-Antarctic South Atlantic (Ocean Drilling Program Site 1089). J. Geophys. Res. 108, 2244, doi:10.1029/2001JB001390.
Stoner, J.S., Laj, C., Channell, J.E.T., Kissel, C., 2002. South Atlantic and North Atlantic geomagnetic paleointensity stacks (0–80 ka); implications for inter-hemispheric correlation. Quat. Sci. Rev. 21, 1141–1151.
Tauxe, L., 1993. Sedimentary records of relative paleointensity of the geomagnetic field: theory and practice. Rev. Geophys. 31, 319–354.
Tauxe, L., Shackleton, N.J., 1994. Relative palaeointensity records from the Ontong-Java Plateau. Geophys. J. Int. 117, 769–782.
Tauxe, L., Steindorf, J.L., Harris, A., 2006. Depositional remanent magnetization; toward an improved theoretical and experimental foundation. Earth Planet. Sci. Lett. 244, 515–529.
Tauxe, L., Wu, G., 1990. Normalized remanence in sediments of the western Equatorial Pacific: relative paleointensity of the geomagnetic field? J. Geophys. Res. 95, 12337–12350.
Thouveny, N., Carcaillet, J., Moreno, E., Leduc, G., Nerini, D., 2004. Geomagnetic moment variation and paleomagnetic excursions since 400 kyr BP: a stacked record from sedimentary sequences of the Portuguese margin. Earth Planet. Sci. Lett. 219, 377–396.
Tilgner, A., 2005. Precession driven dynamos. Phys. Fluids 17, 034014, doi:10.1063/1.1852576.
Tilgner, A., 2007. Kinematic dynamos with precession driven flow in a sphere. Geophys. Astrophys. Fluid Dyn. 101, 1–9.
Torrence, C., Compo, G.P., 1998. A practical guide to wavelet analysis. Bull. Am. Meteor. Soc. 79, 61–78.
Torrence, C., Webster, P.J., 1999. Interdecadal changes in the ENSO-monsoon system. J. Climate 12, 2679–2690.
Valet, J.-P., Meynadier, L., 1993. Geomagnetic field intensity and reversals during the past four million years. Nature 366, 234–238.
Valet, J.P., 2003. Time variations in geomagnetic intensity. Rev. Geophys. 41, 1004, doi:10.1029/2001RG000104.
Vanyo, J.P., Dunn, J.R., 2000. Core precession: flow structures and energy. Geophys. J. Int. 142, 409–425.
Venuti, A., Florindo, F., Michel, E., Hall, I.R., 2007. Magnetic proxy for the deep (Pacific) western boundary current variability across the mid-Pleistocene climate transition. Earth Planet. Sci. Lett. 259, 107–118.
Wagner, G., Beer, J., Laj, C., Kissel, C., Masarik, J., Muscheler, R., Synal, H.A., 2000. Chlorine-36 evidence for the Mono Lake event in the Summit GRIP ice core. Earth Planet. Sci. Lett. 181, 1–6.
Winterwerp, J.C., Kesteren, W.G.M.V., 2004. Introduction to the physics of cohesive sediments in the marine environment. Developments in Sedimentology, vol. 56. Elsevier, Amsterdam.
Wu, C.C., Roberts, P.H., 2008. A precessionally-driven dynamo in a plane layer. Geophys. Astrophys. Fluid Dyn. 102, 1–19.
Xuan, C., Channell, J.E.T., 2008. Testing the relationship between timing of geomagnetic reversals/excursions and phase of orbital cycles using circular statistics and Monte Carlo simulations. Earth Planet. Sci. Lett. 268, 245–254.
Yamazaki, T., 1999. Relative paleointensity of the geomagnetic field during Brunhes Chron recorded in North Pacific deep-sea sediment cores: orbital influence? Earth Planet Sci. Lett. 169, 23–35.
Yamazaki, T., Oda, H., 2002. Orbital influence on Earth's magnetic field: 100,000-year periodicity in inclination. Science 295, 2435–2438.
Yamazaki, T., Oda, H., 2005. A geomagnetic paleointensity stack between 0.8 and 3.0 Ma from Equatorial Pacific sediment cores. Geochem. Geophys. Geosyst. 6, Q11H20, doi:10.1029/2005GC001001.
Yokoyama, Y., Yamazaki, T., 2000. Geomagnetic paleointensity variation with a 100 kyr quasi-period. Earth Planet. Sci. Lett. 181, 7–14.
Yokoyama, Y., Yamazaki, T., Oda, H., 2007. Geomagnetic 100-kyr variation extracted from paleointensity records of the equatorial and north pacific sediments. Earth Planets Space 59, 795–805.